

Experimental investigation and model development for effective viscosity of Al₂O₃-glycerol nanofluids by using dimensional analysis and GMDH-NN methods

Mohsen Sharifpur*, Saheed Adewale Adio, and Josua Petrus Meyer

Department of Mechanical and Aeronautical Engineering, University of Pretoria, Pretoria 0002, South Africa.

Abstract

Nanofluids are new heat transfer fluids which aimed to improve the poor heat removal efficiency of conventional heat transfer fluids. The dispersion of nanoparticles into traditional heat transfer fluids such as ethylene glycol, glycerol, engine oil, gear oil and water has become widely applicable in engineering systems because of their superior heat transfer properties. However, viscosity increase due to nanoparticle dispersion is an issue which needs attention and proper experimental investigation. Therefore, in this study, it is experimentally optimized the two-step preparation procedure for Al₂O₃-glycerol nanofluids consisting of 19, 139 and 160 nm particle sizes, and then studied the effective viscosity between 20-70 °C for the range of 0 to 5% volume fractions. The nanofluids' viscosity showed a characteristic increase as volume fraction increases; decrease as the working temperature increases; and the smallest nanoparticles showed the highest shear resistance. Based on the available experimental data, an empirical correlation has been offered using dimensional analysis. Thereafter, a hybrid neural network based on the group method of data handling (GMDH-NN) has been employed for modeling the effective viscosity of Al₂O₃-glycerol nanofluid. The correlations obtained from both modeling procedures showed higher accuracy in the prediction of the present experimental data when compared to most cited models from the open literature.

Keywords: Nanofluid, Viscosity, Al₂O₃-glycerol, GMDH, Neural network

Nomenclature

a_i	grand model coefficient
A	absorbance
d	characteristic size of a nanoparticle (nm)
h	capping layer thickness (nm)
N	number of independent variable
I	light intensity of UV-vis
l	length of the optical path

* E-mail: Mohsen.Sharifpur@up.ac.za

Tel: +27 12 4202448

M	number of data points used for network training
$\frac{=}{p}$	fitting parameters
\mathfrak{R}	system parameter
T	working temperature (°C)
T_0	reference temperature (°C)
x	data point
y	GMDH model output
Y	adjustable parameter

Greek symbols

α	empirical constant
β	empirical constant
γ	empirical constant
ε	molar absorptivity
$[\eta]$	intrinsic viscosity
μ_{eff}	effective viscosity of nanofluid (mPa.s)
μ_o	viscosity of base fluid (mPa.s)
μ_r	relative viscosity
ρ_{nf}	density of nanofluid (kg/m ³)
ρ_o	density of base fluid (kg/m ³)
ϕ	volume fraction/concentration

Subscripts

0	reference
m	maximum
nf	nanofluid
o	base fluid

Abbreviation

APS	average particle size
GA-GMDH	genetic algorithm-group method of data handling
GMDH	group method of data handling
GMDH-NN	group method of data handling-neural network
JCPDS	joint committee on powder diffraction standards
MAE	mean absolute error
RMSE	root mean square error

SSE	sum of squared errors
TEM	transmission electron microscope
XRD	X-ray diffraction

1. Introduction

The demand for effective heat transfer in engineering systems has increased exponentially with regards to the recent miniaturization of devices and technological advancements. Consequently, different methodologies have been proposed and investigated for managing the associated thermal management challenges. However, the use of modified heat transfer fluid (nanofluid) has become applicable and is currently being investigated for use in refrigeration and air-conditioning systems; boiling and condensation heat transfer; lubrication, transportation systems, Bioengineering, therapeutics and electronics devices [1–4]. The dispersion of nanoparticles into conventional heat transfer fluids such as ethylene glycol, glycerol, engine oil, gear oil and water are of special interest due to their reported unique behaviors [5–7]. It is a known fact that conventional heat transfer fluids are characteristically poor in thermal properties [8,9]. Moreover, several studies [10–13] have shown that the addition of nanoparticles to these conventional heat transfer fluids increases their thermal conductivity, heat capacity, electrical conductivity and convective heat transfer coefficient when used in flow equipment. Although, the underlying factors are controversial and still a subject of investigation.

There are vast areas of applications of nanofluids and as a result, several researchers have paid attention to the different areas of their application. Some major contributions have been made in the area of thermofluids engineering and these contributions have been reported in the literature. Gowda et al. [8] showed that the enhancement in the thermal conductivity of nanofluids is dependent on nanoparticle type, nanoparticle volume fraction, nanoparticles surface charge, base fluid type and the overall energy input into the nanofluid preparation. Other researchers have shown that the thermal properties of nanofluid are also dependent on temperature and the particle size, the use of dispersant and type of dispersion assist mechanism used for the preparation [14–16]. Research works have also been carried out on the electrical conductivity of nanofluids [17–19], rheology and viscosity of nanofluids [20,21], and convective heat transfer using nanofluids [12,22]. Mostly investigated thermophysical properties of nanofluids are the thermal conductivity and the convective heat transfer coefficient. Viscosity is rarely the focus of most research works despite its importance in heat transfer processes, especially those involving fluid flows. Reynolds and Prandtl numbers are two very important non-dimensional numbers that are strongly dependent on the viscosity of working fluid. Increase in viscosity leads to increase in pumping power requirement for forced convection processes; and in situations where natural convection is required, it may increase the system's core temperature due to poor convection current. Therefore, the idea is to find the optimum condition for each nanofluid while, for example by increasing volume fraction or decreasing the particle size the thermal conductivity of a nanofluid increases (advantage) as well as the viscosity (disadvantage). This shows for heat transfer application, the viscosity of nanofluids is as important as the

thermal conductivity is. Thus, an effort to accurately predict nanofluid viscosity is very crucial so that viscosity characteristics will be known before hand and also the ratio of the effective thermal conductivity to viscosity can be determined and analyzed to see the engineering applicability of the nanofluid [23].

Liquid with very low freezing point temperature is desirable as heat transfer fluid in different equipment for building heating and ventilation systems, especially, in cold regions of the world. Such liquid as ethylene glycol or glycerol are either mixed in ratio with other low viscosity fluids or used directly as the working fluid for this kind of applications. Generally, glycerol is used as an additive in many cosmetic products such as hair cream and body lotions due to its hygroscopic ability on moisturized surface. Recently, the ASTM under the theme “*research and long range planning*” is developing standards and considering the replacement of ethylene glycol with glycerol for use as antifreeze in automobile, light duty service and heavy duty engines [24]. This consideration is based on the environmental friendliness and abundance of glycerol compared to the currently used ethylene glycol. More importantly, glycerol is good at resisting oxidation than general lubricant oil, which is why it is a good choice for lubrication as well.

In view of the special properties of glycerol and its economic sustainability viewpoint, together with the fact that Al_2O_3 nanoparticles is one of the most used nanoparticles for nanofluidic applications, it was thought necessary to study the viscosity evolution of Al_2O_3 -glycerol nanofluids. Consideration will be given to different particle sizes, volume fractions and temperatures as the input parameters. Li et al. [25] reported the methods of preparation of nanofluids and their characterization. This is a very key subject in nanofluids development; however, it is yet to receive the much needed attention. Therefore, in this communication, the nanofluid samples were prepared through optimized ultrasonication assisted two-step method. The obtained experimental data are further discussed in view of the several models for the viscosity of nanofluids available in the literature and correlations based on both dimensional analysis with regression and the group method of data handling (GMDH)-neural network is developed.

2. Experimental

In this work, three different sizes of Al_2O_3 nanoparticles were used, namely: 20-30 nm procured from Nanomaterials Inc., 80 nm procured from MK Nano and 100 nm procured from US Nanomaterials Inc. All nanoparticle samples came with true density of 3.7 g/cm^3 . The nanoparticles were characterized using both transmission electron microscope (TEM) imaging (JEOL JEM-2100F) and X-ray diffraction (XRD) pattern (PANalytical XPERT-PRO diffractometer). The nanofluid samples were also characterized using UV-visible (UV-vis) light spectrophotometer (Model 7315 from Jenway). The investigation was done for nanoparticles volume fractions up to 5% where the nanofluids were prepared by the two-step method and sonification. Therefore, the mixture was homogenized using a 200 Watt, 24 kHz Hielscher ultrasonic processor (UP200S) at energy densities ranging from $1.5 \times 10^6 - 4.0 \times 10^7 \text{ kJ/m}^3$. Viscosity measurement was carried out using a vibro-viscometer (SV-10) with a water jacket sampling cup. The sampling cup was connected to a constant temperature thermal bath (LAUDA ECO RE1225 Silver). The viscometer

was calibrated and tested using a fluid of known viscosity. Fig. 1 shows the experimental setup for both the nanofluid preparation and viscosity measurement. More details on the experimental procedure is provided elsewhere [11]. The measurements were carried out in the temperature range of 20-70 °C.

3. Experimental results

TEM image for the nanoparticle samples used in the present work is shown in Fig. 2 (a, c and e). The corresponding size analysis is also as shown in Fig. 2 (b, d, and f). The 20-30 nm gave average particle size (APS) of 19 nm, the 80 nm gave APS of 160 nm (different than the manufacturer claim) and the 100 nm gave APS of 139 nm. Hence, throughout the rest of this paper the size of these nanoparticles will be taken as the actual measured of 19, 139 and 160 nm. In Fig. 3 (a) the XRD peaks pattern was identified as Al_2O_3 with traces of $\text{Al}_2(\text{SO}_4)_3$ both corresponding to 01-083-2080 and 01-077-0385 file numbers from the joint committee on powder diffraction standards (JCPDS). The nature of the diffraction peaks in Fig. 3 (a) indicates that the 19 nm sample is in amorphous phase, while Fig. 3 (b, c) peaks patterns show that the 139 and 160 nm samples are in crystalline form. Also the peaks matched Al_2O_3 with traces of $\text{Al}_2(\text{SO}_4)_3$ (JCPDS file numbers: 01-081-2267 and 01-077-0066) for 139 nm and Al_2O_3 (JCPDS file number: 90-008-8029) for 160 nm.

The UV-vis spectra pattern for all the nanofluids at different volume fraction from 0.01% to 0.035% are presented in Fig. 4. Very low volume fractions were chosen for the UV-vis experiment because at a higher volume fraction the absorbance were out of the range for the spectrophotometer. The UV-vis analysis is of the convenient ways to characterize the dispersion of nanofluid. Using the Beer Lambert law presented in Eq. (1), the light absorbency ratio index of the nanofluid can be calculated:

$$A = -\log \frac{I_o}{I} = \varepsilon l \phi \quad (1)$$

In Eq. (1), A is the absorbance, I_o is the intensity of the UV-vis light through the blank, I is the intensity of the UV-vis light through the samples, ε is the molar absorptivity, l is the optical path which is the length of test section light passes through and ϕ is the concentration of the particles in suspension. The equation shows that at fixed optical path and molar absorptivity, the absorbency of a suspension is proportional to the concentration of the particles in the suspension. Fig. 4 (a, b and c) shows the UV-vis spectra of Al_2O_3 -glycerol nanofluids for different concentrations. The UV-vis spectra of Al_2O_3 -glycerol nanofluids featured a strong absorption band at around 230 nm wavelength followed by a monotonic decrease in absorbance when increasing wavelength. The spectra pattern and the strongest peak wavelength corresponds to previous analysis carried out by Piriya Wong et al. [26] on Al_2O_3 dispersed in deionized water. In Fig. 4 (d, e and f), it is clear that the absorbance increases as the nanoparticle concentration increases. It should also be noted that as the absorbance increases with increasing the amount of dispersed (Al_2O_3), it shows good dispersion of nanoparticle in the base fluid if the relationship is linear following the Beer's law Fig. 4 (d, e and f) [27].

The nanoparticles were sonicated by applying different energy densities ranging from $1.5.0 \times 10^6$ – 4.0×10^7 kJ/m^3 . This was done to identify which energy density can provide better dispersion for effective viscosity measurement. The use of rheology to characterize the state of dispersion of nanostructures in base fluid materials is a well-known procedure and has been applied in the past [28, 29]. Using this procedure the nanofluid will be sonicated applying different energy inputs and the viscosity of the sample will be monitored until the viscosity gets minimized. Fig. 5 shows the influence of ultrasonication energy density on the effective viscosity of the Al_2O_3 -glycerol nanofluids. In the 19 nm sample the nanofluid became uniformly dispersed at 3.0×10^7 kJ/m^3 energy density because the viscosity does not change with further ultrasonication. While for the nanofluid samples prepared from 139 and 160 nm nanoparticles, the viscosity was minimum at 1.5×10^6 kJ/m^3 energy density. The increase in viscosity of 139 nm Al_2O_3 samples as seen in Fig. 5 is due to the prolonged ultrasonication period, which led the particles to coalesce and reform loose aggregates that allow the entrapment of fluid and cause increased viscosity as previously reported by Enomoto *et al.* [30] and, Suganthi and Rajan [31]. Lower nanoparticle size required higher ultrasonication energy to bring them to uniform homogenization due to increased particle-particle interaction that enhances aggregation. The results presented below are therefore based on uniformly homogenized nanofluids.

In order to highlight the effect of temperature on the effective viscosity of the nanofluids samples, the measured effective viscosities at various volume fractions have been plotted against temperature in Fig. 6. The effective viscosity of the nanofluids decreases as the temperature increases, with a decreasing slope and displayed asymptotic feature. The trend of the curves is noticed to be similar in all cases across all particle sizes and volume fractions. In the Fig. 6, the curve of the viscosity of pure glycerol is provided for comparison and it is noticed that the difference between the effective viscosity of the nanofluid and that of pure glycerol reduces as the temperature increases. This is primarily due to the influence of the temperature in the weakening of the intermolecular bonding which drastically reduced the shear resistance of the nanofluid samples. The relative viscosity of Al_2O_3 -glycerol nanofluids at different volume fractions as a function of the working temperature is presented in Fig. 7. It can be noted that irrespective of the nanoparticle volume fraction, the relative viscosity maintained almost constant across the temperature regime. This has an exception for the case of 5% volume fraction of 19 nm sample which can be attributed to the increase in particle-particle interactions at higher volume fraction. It is noteworthy that the number density of particles present at 5% of 19 nm is much more than 5% of 139 nm as well as 5% of 160 nm, therefore, the observed deviation is the cumulative effect of small particle size, effective volume fraction and Brownian motion at higher working temperature. Similar results regarding the behavior of the relative viscosity of other nanofluids with respect to temperature increase have been previously reported [32–34].

Fig. 8 shows the influence of volume fraction on the relative viscosity of all the nanofluid samples investigated. As expected, the relative viscosity of the nanofluids increased with increase in volume

fraction nonlinearly. This behavior is typical for nanofluids viscosity [35]. Regarding the influence of particle size, the agreement is that the smaller the particle size the higher the viscosity of the nanofluid [36,37]. Moreover, there are different parameters to be considered when discussing nanofluids viscosity. They include volume fraction, base fluid characteristics (polar, nonpolar, Newtonian and non-Newtonian), experimental techniques, the pH of the nanofluid and especially nanoparticle properties such as size, shape and size distribution as well as how to produce the nanoparticle or nanofluids (one step or two-step) [33,36–39]. In the present study, the nanofluid samples based on 19 nm Al₂O₃ showed the highest viscosity followed by 139 nm Al₂O₃ and lowest values were recorded in nanofluid samples based on 160 nm Al₂O₃. This behavior is consistent with reported trends for other nanofluids (e.g. SiC-water and SiO₂-water) concerning the particle size influence [36, 37]. The same principle of number density mentioned above still plays a significant role in the observed viscosity values. As the particle size increases, the number of particles and the total surface area of the liquid-solid interface at a given volume fraction reduces. This reduces the electro-viscous effect as a result of reduced particle-liquid interaction in comparison to smaller particle size that has higher effective volume fraction due to higher number density [36]. Also, the electro-viscous interaction between the particles (which is called the second electro-viscous effect) reduces as particle size increases. Thus, nanofluid samples from bigger MgO particle size showed lower resistance to flow due to reduced particle-particle and particle-fluid interactions.

Modeling

As stated in the discussion above, there are several factors affecting the viscosity of nanofluid, however, most prominently investigated are temperature, volume fraction and particle size. Many developed theoretical and empirical models in the past only consider the effect of either one of these aforementioned factors. For instance, the work of Einstein [40] on infinite dilute suspension of uncharged, hard solid spheres in liquid medium was the first presented theoretical work on the viscosity of suspensions that gave the model in Eq. (2):

$$\mu_{eff} = \mu_o (1 + [\eta]\phi) \quad (2)$$

In the above expression μ_{eff} is the effective viscosity of the colloid, μ_o is the dynamic viscosity of the suspending medium, ϕ is the particle volume fraction and $[\eta]$ is the intrinsic viscosity of the suspension taken as 2.5. This linear equation of viscosity estimation is based on the assumed absence of interaction between the solid particles and a function of the particle volume fraction only. Einstein's viscosity model may be applicable for estimating suspension viscosity in the dilute regime (volume fraction of $\phi \leq 2\%$).

In reality the dependence of the viscosity of suspensions on the increase of volume fraction is not linear. As opposed to Einstein's assumption of non-interaction of the solid particles, there is constant interaction between particles in suspension due to the presence of Brownian motion [41]. Therefore, to account for the interactions between the particles Brinkman [42] extended Einstein's model for a concentrated particle volume fraction and presented his model as

$$\mu_{eff} = \mu_o \frac{1}{(1-\phi)^{2.5}} \quad (3)$$

Similarly, Roscoe [43] derived the viscosity expression for suspension containing spheres of very diverse sizes and applicable to concentrated suspension. His expression presented in Eq. (4) reduced to Einstein's model in the limit of very dilute volume fractions. Another correlation based on Einstein's model was presented by Batchelor [44]. Batchelor [44] considered the Brownian interactions between spherical particles to derive the viscosity expression presented in Eq. (5):

$$\mu_{eff} = \mu_o (1-\phi)^{-2.5} \quad (4)$$

$$\mu_{eff} = \mu_o (1 + 2.5\phi + 6.2\phi^2) \quad (5)$$

The increased interaction rate between suspended particles at high volume fractions often lead to agglomeration of the particles which the earlier theoretical models did not consider. Krieger and Dougherty [45] considered the crowding effects due to interactions of solid particles to arrive at the model expression in Eq. (6) which is a modified form of Mooney's functional analysis:

$$\mu_{eff} = \mu_o \left(1 - \frac{\phi}{\phi_m}\right)^{-[\eta]\phi_m} \quad (6)$$

where ϕ_m is the maximum packing fraction. Kitano et al. [46] suggested a simple expression for the prediction of effective viscosity based on Maron-Pierce's equation. In their correlation which is presented in Eq. (7), μ_r is the relative viscosity and it was determined for the application of equal shear stress to the suspensions:

$$\mu_r = \left(1 - \frac{\phi}{Y}\right)^{-2} \quad (7)$$

where Y is an adjustable parameter based on the following expression: $Y = 0.54 - 0.0125\bar{p}$ and \bar{p} is a form of fitting parameter. It is noteworthy that there are numerous other mathematical models that also have been developed considering only temperature [47–49].

4.1 Dimensional analysis

In the present work, temperature, volume fraction, particle size, capping layer thickness, base fluid viscosity, nanofluid density and base fluid density were all considered to have significant influence on the effective viscosity of nanofluid. Using dimensional analysis, the factors were reduced to non-dimensional parameters given in the Eq. (8):

$$\pi_1 = \frac{\mu_{eff}}{\mu_o} = f\left(\pi_2 = \frac{T}{T_0}, \pi_3 = \phi, \pi_4 = \frac{d}{h}, \pi_5 = \frac{\rho_{nf}}{\rho_{bf}}\right) \quad (8)$$

In the Eq. (8) above, T is the working temperature, d is the particle diameter, ρ_{nf} is the density of nanofluid, ρ_{bf} is the density of base fluid, T_0 is the reference temperature taken as 20 °C and h is the thickness of the capping layer taken as 1 nm [50]. The densities of the nanofluids were calculated based on the mixture model [51] and correlation matrix was run on 132 data points for all the four independent non-dimensional parameters. The result of the correlation matrix shows that π_3 and π_5 are highly correlated with 99.96%. Since the volume fraction (π_3) is part of the variable parameters in the present work, this takes precedence over π_5 . Therefore, Eq. (8) is reduced to Eq. (9):

$$\frac{\mu_{eff}}{\mu_o} = f\left(\frac{T}{T_0}, \phi, \frac{d}{h}\right) \quad (9)$$

Using regression modeling, the function f in Eq. (9) is expressed as

$$\frac{\mu_{eff}}{\mu_o} = 1 + \Re[\eta] \cdot \left[\left(\frac{T}{T_0}\right)^\alpha \cdot \phi^\beta \cdot \left(\frac{d}{h}\right)^\gamma \right] \quad (10)$$

where \Re is the system parameter, $[\eta]$ is the intrinsic viscosity, α , β , and γ are correlation coefficients. The system parameter (\Re) and correlation coefficients (α , β , and γ) for this model are as 240.19, 0.807, 2.480 and -0.522, respectively. The parity plot between the predicted results and the experimental data of Eq. (10) is shown in Fig. 9. The predicted results using this model show maximum deviation of about $\pm 15\%$ from the experimental observations. Table 1 shows the statistics on the accuracy of the model. Although the coefficient of determination (R^2) of this model is 0.9495, however, the model still outperforms the most cited theoretical and empirical models in the prediction of the present experimental data as explained below. Presented in Fig. 10 is the comparison between the viscosity ratios of Al₂O₃-glycerol nanofluids obtained from the current experiment, the dimensionless empirical correlation based on the current experimental data and some of the several models reported in the literature. These models used for comparison are selected because of their high level of acceptability and citation in nanofluid research field. Besides, most of the empirical models developed were missing some of the input parameters such as size and temperature, while others do not give the value of the base fluid when there is no nanoparticle addition. For example the model of Hosseini et al. [50] has all the three parameters as investigated in this work (size, volume fraction and temperature) and it was developed for Al₂O₃-water nanofluids, however, when $\phi = 0$ the model failed to return the base fluid viscosity value and when applied to the present data it does not give good correlation results. As shown in the Fig. 10, the model in Eq. (10) predicted the experimental data fairly well, unlike the previously published models. The main cause of the difference between the experimental data and the previously published models is because most of the models are based on low concentration and micron size particle. Moreover, particle size and temperature were never considered in these models and this may hinder the applicability of the models.

4.2 Neural network

The group method of data handling (GMDH) algorithm was first introduced by Ivankhnenko [52] as a learning algorithm to perform generation and selection of model structures based on the neurons that give optimized output. However, numerous researchers have formulated different hybrid network systems based on the GMDH algorithms such as genetic algorithm-GMDH-type polynomial neural network (GA-GMDH) by Mehrabi et al. [53] and GMDH- type polynomial neural network (GMDH-PNN) by Atashrouz et al. [54]. This is because the initial GMDH algorithm by Ivankhnenko was limited in terms of the number of independent input variable that can be combined at a time during the iterative procedure. This limitation reduced the complexity and accuracy of the algorithm to predict non-linear systems.

Since the viscosity data in the present work are nonlinear with consideration given to the following effective parameters; particle size, temperature and volume fraction, a hybrid GMDH-type neural network (GMDH-NN) achieved by combining GMDH and artificial neural network was used to model the experimental data. This type of network is based on the formation of several layers from the combination of two or more input variables and has several neurons in each layer. This hybrid GMDH-NN uses the combinatorial algorithm to optimize the connections between the neurons in each layer. The established relationship between every input and output into the neurons at every stage of the iteration is a multinomial expression in the form of Eq. (11) known as Volterra-Kolmogorov-Gabor function.

$$y_i = a + \sum_{i=1}^N a_i x_i + \sum_{i=1}^N \sum_{j=1}^N a_{ij} x_i x_j + \sum_{i=1}^N \sum_{j=1}^N \sum_{k=1}^N a_{ijk} x_i x_j x_k + \dots \quad (11)$$

where N is the number of independent variables, $a_{i,j,\dots}$ are the unknown coefficients or weights and x_i, x_j, x_k are the independent variables. In GMDH-NN, the Volterra-Kolmogorov-Gabor neuron function is disintegrated into quadratic polynomial of the form in Eq. (12) and the coefficients are determined using the method of the least square approximation. The deviation between the experimental data and the GMDH-NN predicted results is monitored using both the mean absolute error (MAE) and root mean square error (RMSE) as in Eq. (13) and Eq. (14) as statistical tools.

$$f_i(x_i, x_j) = a_0 + a_1 x_i + a_2 x_j + a_3 x_i x_j + a_4 x_i^2 + a_5 x_j^2 \quad (12)$$

$$MAE = \frac{1}{M} \sum_{i=1}^M \left(\left| \frac{\mu_{eff}}{\mu_o} \right|_{Exp} - \left| \frac{\mu_{eff}}{\mu_o} \right|_{pred} \right) \quad (13)$$

$$RMSE = \sqrt{\frac{1}{M} \sum_{i=1}^M \left(\left| \frac{\mu_{eff}}{\mu_o} \right|_{Exp} - \left| \frac{\mu_{eff}}{\mu_o} \right|_{pred} \right)^2} \quad (14)$$

It should be noted that the experimental data are divided into two sets (training and testing sets). The coefficient in Eq. (12) are fitted using the training data set, while the testing data is used to select the most accurate model combination that satisfies the eternal criterion. A set of 132 experimental data points on

the viscosity of Al₂O₃-glycerol nanofluids was employed in which each of them containing input parameters of particle size, temperature and volume fraction.

The GMDH-NN system provided a system of polynomial after it was executed using a random 60% of the data for training and the rest 40% used to validate the system. The proposed GMDH-NN grand model is presented in appendix A. A parity plot between the GMDH-NN predicted results and the experimental data is presented in Fig. 11. It is clear from the figure that the predicted results are at par with experimentally observed data and the model's R², is 0.9905. Other statistics on the accuracy of the model are presented in Table 1. Fig. 12 shows the performance of the GMDH-NN in predicting the viscosity of Al₂O₃-glycerol nanofluid with respect to temperature and volume fraction. The GMDH-NN model showed very good agreement with the experimental data for the independent parameters considered. Considering the statistics provided the Table 1, the GMDH-NN model is more accurate than the dimensional analysis model. However, the model in Eq. (10) is more user friendly and less complex, especially when it is needed to introduce the formulation in a computational fluid dynamic simulation where the nanofluid is employed as a heat transfer fluid.

Conclusion

In this study, the two-step method of nanofluid preparation, assisted with ultrasonication was optimized in order to obtain a uniformly homogenized suspension. Thereafter, the influence of temperature, particle size and volume fraction on the effective viscosity of Al₂O₃-glycerol nanofluid was investigated. The nanofluids viscosity showed a characteristic increase with volume fraction increase; decrease with the working temperature increase; and the smallest nanoparticles showed very high shear resistance. Using the present experimental data, an empirical model based on dimensional analysis was proposed. Furthermore, a hybrid GMDH-NN algorithm was also employed for modeling the effective viscosity of Al₂O₃-glycerol nanofluids. The correlations obtained from both modeling procedures showed higher accuracy in the prediction of the present experimental data when compared to Einstein's, Batchelor's, Krieger-Dougherty's and Kitano's models.

Appendix A

The GMDH-NN grand model.

$$\begin{aligned}
 \mu_r &= a_{17,0} + a_{11,1} \cdot N_{11} + a_{17,2} \cdot N_{11} \cdot N_{18} + a_{17,3} \cdot N_{11}^2 + a_{17,4} \cdot N_{18}^2 \\
 N_{11} &= a_{1,0} + a_{1,1} \cdot \left(\frac{T}{T_0}\right) + a_{1,2} \cdot N_{25} \cdot \left(\frac{T}{T_0}\right) + a_{1,3} \cdot \left(\frac{T}{T_0}\right)^2 + a_{1,4} \cdot N_{25} \\
 N_{18} &= a_{2,0} + a_{2,1} \cdot N_{35} + a_{2,2} \cdot N_{35} \cdot N_{41} + a_{2,3} \cdot N_{35}^2 + a_{2,4} \cdot N_{41} \\
 N_{25} &= a_{3,0} + a_{3,1} \cdot N_{53} + a_{3,2} \cdot N_{53} \cdot N_{63} + a_{3,3} \cdot N_{53}^2 + a_{3,4} \cdot N_{63} \\
 N_{35} &= a_{4,0} + a_{4,1} \cdot N_{74} + a_{4,2} \cdot N_{49} \cdot N_{74} + a_{4,3} \cdot N_{74}^2 + a_{4,4} \cdot N_{49} + a_{4,5} \cdot N_{49}^2 \\
 N_{41} &= a_{5,0} + a_{5,1} \cdot N_{58} + a_{5,2} \cdot N_{58} \cdot N_{68} + a_{5,3} \cdot N_{58}^2 + a_{5,4} \cdot N_{68} + a_{5,5} \cdot N_{68}^2 \\
 N_{49} &= a_{6,0} + a_{6,1} \cdot N_{74} + a_{6,2} \cdot N_{74} \cdot N_{78} + a_{6,3} \cdot N_{74}^2 + a_{6,4} \cdot N_{78}^2 \\
 N_{53} &= a_{7,0} + a_{7,1} \cdot \left(\frac{d}{h}\right) + a_{7,2} \cdot N_{77} \cdot \left(\frac{d}{h}\right) + a_{7,3} \cdot N_{77} + a_{7,4} \cdot N_{77}^2 \\
 N_{58} &= a_{8,0} + a_{8,1} \cdot \left(\frac{T}{T_0}\right) + a_{8,2} \cdot N_{74} \cdot \left(\frac{T}{T_0}\right) + a_{8,3} \cdot \left(\frac{T}{T_0}\right)^2 + a_{8,4} \cdot N_{74} + a_{8,5} \cdot N_{74}^2 \\
 N_{63} &= a_{9,0} + a_{9,1} \cdot \left(\frac{d}{h}\right) + a_{9,2} \cdot N_{79} \cdot \left(\frac{d}{h}\right) + a_{9,3} \cdot N_{79} + a_{9,4} \cdot N_{79}^2 \\
 N_{68} &= a_{10,0} + a_{10,1} \cdot N_{80} + a_{10,2} \cdot N_{80} \cdot N_{88} + a_{10,3} \cdot N_{80}^2 + a_{10,4} \cdot N_{88} \\
 N_{74} &= a_{11,0} + a_{11,1} \cdot \phi + a_{11,2} \cdot \phi \cdot \left(\frac{d}{h}\right)^{\frac{1}{3}} + a_{11,3} \cdot \phi^2 + a_{11,4} \cdot \left(\frac{d}{h}\right)^{\frac{1}{3}} \\
 N_{77} &= a_{12,0} + a_{12,1} \cdot \phi + a_{12,2} \cdot \phi \cdot \left(\frac{T}{T_0}\right)^{\frac{1}{3}} + a_{12,3} \cdot \phi^2 + a_{12,4} \cdot \left(\frac{T}{T_0}\right)^{\frac{1}{6}} \\
 N_{78} &= a_{13,0} + a_{13,1} \cdot \phi + a_{13,2} \cdot \phi \cdot \left(\frac{T}{T_0}\right) + a_{13,3} \cdot \phi^2 + a_{13,4} \cdot \left(\frac{T}{T_0}\right)^2 \\
 N_{79} &= a_{14,0} + a_{14,1} \cdot \phi^{\frac{1}{3}} + a_{14,2} \cdot \left(\frac{\phi \cdot T}{T_0}\right)^{\frac{1}{3}} + a_{14,3} \cdot \phi^{\frac{1}{6}} + a_{13,4} \cdot \left(\frac{T}{T_0}\right)^{\frac{1}{6}} \\
 N_{80} &= a_{15,0} + a_{15,1} \cdot \left(\frac{T}{T_0}\right) \cdot \phi^{\frac{1}{3}} + a_{15,2} \cdot \left(\frac{T}{T_0}\right)^2 + a_{15,3} \cdot \phi^{\frac{1}{3}} + a_{15,4} \cdot \phi^{\frac{1}{6}} \\
 N_{88} &= a_{16,0} + a_{16,1} \cdot \left(\frac{d}{h}\right)^{\frac{4}{3}}
 \end{aligned}$$

$$[\bar{a}_{i,j}] = \begin{bmatrix}
 -0.321517 & 0.25606 & -0.0370338 & -0.048751 & 1.10191 & 0 \\
 -0.188348 & 1.23044 & 4.49926 & -2.41921 & -2.13299 & 0 \\
 -0.140132 & -2.75747 & -4.79704 & 4.70576 & 3.99177 & 0 \\
 -0.0307418 & 0.538185 & -1.53936 & 0.598807 & 0.55801 & 0.880023 \\
 0.173143 & -1.92998 & -15.5739 & 8.5577 & 2.74038 & 7.14322 \\
 1.49413 & -1.27825 & 2.71316 & -0.68996 & -1.17788 & 0 \\
 -0.935389 & 1.15697 & -1.0292 & 1.69105 & 0.127347 & 0 \\
 1.43738 & -0.300686 & 0.381542 & -0.0263996 & -0.649262 & 0.228859 \\
 -0.482389 & 1.13287 & -1.0101 & 1.0606 & 0.331032 & 0 \\
 7.83947 & -6.43514 & 4.69425 & 0.384991 & -5.25237 & 0 \\
 0.255487 & 42.7945 & -49.5965 & 423.808 & 0.829561 & 0 \\
 1.30942 & -45.7755 & 33.4417 & 399.686 & -0.168446 & 0 \\
 1.14943 & -18.5889 & 7.06931 & 400.59 & -0.0217554 & 0 \\
 4.53686 & -30.2614 & 8.01848 & 43.5546 & -0.725447 & 0 \\
 3.7242 & 1.4423 & -0.0709741 & -23.2172 & 43.6259 & 0 \\
 1.53855 & -0.173113 & 0 & 0 & 0 & 0 \\
 0.00719965 & 0.968948 & 13.6328 & 6.65067 & 6.99027 & 0
 \end{bmatrix}$$

Acknowledgments

The authors gratefully acknowledge the funding obtained from the National Research Foundation of South Africa (NRF), Stellenbosch University/University of Pretoria Solar Hub, CSIR, EEDSM Hub, NAC and RDP-seed.

References

- [1] I.M. Mahbubul, S.S. Khaleduzzaman, R. Saidur, M.A. Amalina, Rheological behavior of $\text{Al}_2\text{O}_3/\text{R141b}$ nanorefrigerant, *Int. J. Heat Mass Transf.* 73 (2014) 118–123. doi:10.1016/j.ijheatmasstransfer.2014.01.073.
- [2] M. Kole, T.K. Dey, Thermophysical and pool boiling characteristics of ZnO-ethylene glycol nanofluids, *Int. J. Therm. Sci.* 62 (2012) 61–70. doi:10.1016/j.ijthermalsci.2012.02.002.
- [3] H. Ghaednia, R.L. Jackson, J.M. Khodadadi, Experimental analysis of stable CuO nanoparticle enhanced lubricants, *J. Exp. Nanosci.* 10 (1) (2015) 1–18. doi:10.1080/17458080.2013.778424.
- [4] K. V. Wong, O. De Leon, Applications of Nanofluids: Current and Future, *Adv. Mech. Eng.* 2 (2010) 519659–1–11. doi:10.1155/2010/519659.
- [5] Y.J. Hwang, Y.C. Ahn, H.S. Shin, C.G. Lee, G.T. Kim, H.S. Park, et al., Investigation on characteristics of thermal conductivity enhancement of nanofluids, *Curr. Appl. Phys.* 6 (6) (2006) 1068–1071. doi:10.1016/j.cap.2005.07.021.
- [6] T.T.-K. Hong, H.H.-S. Yang, C.J. Choi, Study of the enhanced thermal conductivity of Fe nanofluids, *J. Appl. Phys.* 97 (064311) (2005) 1–4. doi:10.1063/1.1861145.
- [7] J.A. Eastman, S.U.S. Choi, S. Li, W. Yu, L.J. Thompson, Anomalous increase in effective thermal conductivities of ethylene glycol-based nanofluids containing copper nanoparticles, *Appl. Phys. Lett.* 78 (6) (2001) 718–720. doi:10.1063/1.1341218.
- [8] R. Gowda, H. Sun, P. Wang, M. Charmchi, F. Gao, Z. Gu, et al., Effects of Particle Surface Charge, Species, Concentration, and Dispersion Method on the Thermal Conductivity of Nanofluids, *Adv. Mech. Eng.* 2 (976254) (2010) 1–10. doi:10.1155/2010/807610.
- [9] S.K. Das, N. Putra, P. Thiesen, W. Roetzel, Temperature Dependence of Thermal Conductivity Enhancement for Nanofluids, *J. Heat Transfer.* 125 (4) (2003) 567. doi:10.1115/1.1571080.
- [10] H. Xie, W. Yu, W. Chen, MgO nanofluids: higher thermal conductivity and lower viscosity among ethylene glycol-based nanofluids containing oxide nanoparticles, *J. Exp. Nanosci.* 5 (5) (2010) 463–472. doi:10.1080/17458081003628949.
- [11] S.A. Adio, M. Sharifpur, J.P. Meyer, Investigation Into Effective Viscosity, Electrical Conductivity, and pH of $\gamma\text{-Al}_2\text{O}_3$ -Glycerol Nanofluids in Einstein Concentration Regime, *Heat Transf. Eng.* 36 (14-15) (2015) 1241–1251. doi:10.1080/01457632.2015.994971.
- [12] D.P.D. Kulkarni, P.P.K. Namburu, H. Ed Bargar, D.K. Das, Convective Heat Transfer and Fluid Dynamic Characteristics of SiO_2 Ethylene Glycol/Water Nanofluid, *Heat Transf. Eng.* 29 (12) (2008) 1027–1035. doi:10.1080/01457630802243055.

- [13] M. Ghazvini, E. Rasouli, M. Raisee, Heat Transfer Properties of Nanodiamond – Engine Oil Nanofluid in Laminar Flow of Nanodiamond – Engine Oil Nanofluid in Laminar Flow, *Heat Transf. Eng.* 33 (6) (2012) 525–532. doi:10.1080/01457632.2012.624858.
- [14] M.J. Assael, I.N. Metaxa, K. Kakosimos, D. Constantinou, Thermal Conductivity of Nanofluids – Experimental and Theoretical, *Int. J. Thermophys.* 27 (4) (2006) 999–1017. doi:10.1007/s10765-006-0078-6.
- [15] A. Azari, M. Kalbasi, A. Moazzeni, A. Rahman, A Thermal Conductivity Model for Nanofluids Heat Transfer Enhancement, *Pet. Sci. Technol.* 32 (1) (2014) 91–99. doi:10.1080/10916466.2010.551808.
- [16] A. Amrollahi, A.M. Rashidi, M. Emami Meibodi, K. Kashefi, Conduction heat transfer characteristics and dispersion behaviour of carbon nanofluids as a function of different parameters, *J. Exp. Nanosci.* 4 (4) (2009) 347–363. doi:10.1080/17458080902929929.
- [17] S. Ganguly, S. Sikdar, S. Basu, Experimental investigation of the effective electrical conductivity of aluminum oxide nanofluids, *Powder Technol.* 196 (3) (2009) 326–330. doi:10.1016/j.powtec.2009.08.010.
- [18] A.A. Minea, R.S. Luciu, Investigations on electrical conductivity of stabilized water based Al_2O_3 nanofluids, *Microfluid. Nanofluid.* 13 (6) (2012) 977–985. doi:10.1007/s10404-012-1017-4.
- [19] K.G.K. Sarojini, S. V Manoj, P.K. Singh, T. Pradeep, S.K. Das, Electrical conductivity of ceramic and metallic nanofluids, *Colloids Surfaces A Physicochem. Eng. Asp.* 417 (2013) 39–46. doi:10.1016/j.colsurfa.2012.10.010.
- [20] L. Syam Sundar, E. Venkata Ramana, M.K. Singh, A. C.M. De Sousa, Viscosity of low volume concentrations of magnetic Fe_3O_4 nanoparticles dispersed in ethylene glycol and water mixture, *Chem. Phys. Lett.* 554 (2012) 236–242. doi:10.1016/j.cplett.2012.10.042.
- [21] Y.R. Sekhar, K. V. Sharma, Study of viscosity and specific heat capacity characteristics of water-based Al_2O_3 nanofluids at low particle concentrations, *J. Exp. Nanosci.* 10 (2) (2013) 86–102. doi:10.1080/17458080.2013.796595.
- [22] K.B. Anoop, T. Sundararajan, S.K. Das, Effect of particle size on the convective heat transfer in nanofluid in the developing region, *Int. J. Heat Mass Transf.* 52 (9-10) (2009) 2189–2195. doi:10.1016/j.ijheatmasstransfer.2007.11.063.
- [23] R. Prasher, D. Song, J. Wang, P. Phelan, Measurements of nanofluid viscosity and its implications for thermal applications, *Appl. Phys. Lett.* 89 (133108) (2006) 1–4. doi:10.1063/1.2356113.
- [24] ASTM International, Proposed ASTM Engine Coolant Standards Focus on Glycerin, (2010) 1. <http://www.astmnewsroom.org/default.aspx?pageid=2115>. accessed April, 2015.
- [25] Y. Li, J. Zhou, S. Tung, E. Schneider, S. Xi, A review on development of nanofluid preparation and characterization, *Powder Technol.* 196 (2) (2009) 89–101. doi:10.1016/j.powtec.2009.07.025.

- [26] V. Piriya Wong, V. Thongpool, P. Asanithi, P. Limsuwan, Preparation and characterization of alumina nanoparticles in deionized water using laser ablation technique, *J. Nanomater.* 2012 (2012) 1–6. doi:10.1155/2012/819403.
- [27] M. Mehrali, E. Sadeghinezhad, S.T. Latibari, S.N. Kazi, M. Mehrali, M.N.B.M. Zubir, et al., Investigation of thermal conductivity and rheological properties of nanofluids containing graphene nanoplatelets, *Nanoscale Res. Lett.* 9 (15) (2014) 1–12. doi:10.1186/1556-276X-9-15.
- [28] Y.S. Song, J.R. Youn, Influence of dispersion states of carbon nanotubes on physical properties of epoxy nanocomposites, *Carbon N. Y.* 43 (7) (2005) 1378–1385. doi:10.1016/j.carbon.2005.01.007.
- [29] Y. Yang, E.A. Grulke, Z.G. Zhang, G. Wu, Thermal and rheological properties of carbon nanotube-in-oil dispersions, *J. Appl. Phys.* 99 (11) (2006) 114307-1–8. doi:10.1063/1.2193161.
- [30] N. Enomoto, S. Maruyama, Z. Nakagawa, Agglomeration of silica spheres under ultrasonication, *J. Mater. Res.* 12 (05) (1997) 1410–1415. doi:10.1557/JMR.1997.0192.
- [31] K.S. Suganthi, K.S. Rajan, Temperature induced changes in ZnO–water nanofluid: Zeta potential, size distribution and viscosity profiles, *Int. J. Heat Mass Transf.* 55 (25-26) (2012) 7969–7980. doi:10.1016/j.ijheatmasstransfer.2012.08.032.
- [32] T. Yiamsawas, O. Mahian, A.S. Dalkilic, S. Kaewnai, S. Wongwises, Experimental studies on the viscosity of TiO₂ and Al₂O₃ nanoparticles suspended in a mixture of ethylene glycol and water for high temperature applications, *Appl. Energy.* 111 (2013) 40–45. doi:10.1016/j.apenergy.2013.04.068.
- [33] T. Yiamsawas, A.S. Dalkilic, O. Mahian, S. Wongwises, Measurement and Correlation of the Viscosity of Water-Based Al₂O₃ and TiO₂ Nanofluids in High Temperatures and Comparisons with Literature Reports, *J. Dispers. Sci. Technol.* 34 (12) (2013) 1697–1703. doi:10.1080/01932691.2013.764483.
- [34] D. Singh, E. Timofeeva, W. Yu, J. Routbort, D. France, D. Smith, et al., An investigation of silicon carbide-water nanofluid for heat transfer applications, *J. Appl. Phys.* 105 (6) (2009) 064306-1–6. doi:10.1063/1.3082094.
- [35] S. Bobbo, L. Fedele, A. Benetti, L. Colla, M. Fabrizio, C. Pagura, et al., Viscosity of water based SWCNH and TiO₂ nanofluids, *Exp. Therm. Fluid Sci.* 36 (2012) 65–71. doi:10.1016/j.expthermflusci.2011.08.004.
- [36] E. V Timofeeva, D.S. Smith, W. Yu, D.M. France, D. Singh, J.L. Routbort, Particle size and interfacial effects on thermo-physical and heat transfer characteristics of water-based alpha-SiC nanofluids, *Nanotechnology.* 21 (21) (2010) 215703. doi:10.1088/0957-4484/21/21/215703.
- [37] Z. Jia-Fei, L. Zhong-Yang, Dependence of nanofluid viscosity on particle size and pH value, *Chinese Phys. Lett.* 26 (6) (2009) 10–13.
- [38] E. V. Timofeeva, J.L. Routbort, D. Singh, Particle shape effects on thermophysical properties of alumina nanofluids, *J. Appl. Phys.* 106 (1) (2009) 014304-1–10. doi:10.1063/1.3155999.

- [39] A. Ghadimi, R. Saidur, H.S.C. Metselaar, A review of nanofluid stability properties and characterization in stationary conditions, *Int. J. Heat Mass Transf.* 54 (17-18) (2011) 4051–4068. doi:10.1016/j.ijheatmasstransfer.2011.04.014.
- [40] A. Einstein, A New Determination of Molecular Dimensions, *Ann. Phys.* 4 (19) (1906) 37–62.
- [41] T.S.X. Phuoc, M. Massoudi, Experimental observations of the effects of shear rates and particle concentration on the viscosity of Fe₂O₃-deionized water nanofluids, *Int. J. Therm. Sci.* 48 (7) (2009) 1294–1301. doi:10.1016/j.ijthermalsci.2008.11.015.
- [42] H.C. Brinkman, The viscosity of concentrated suspensions and solutions, *J. Chem. Phys.* 20 (4) (1952) 571.
- [43] R. Roscoe, The viscosity of suspensions of rigid spheres, *J. Appl. Phys.* 267 (1952) 3–6.
- [44] G. Batchelor, The effect of Brownian motion on the bulk stress in the suspension of spherical particles, *J. Fluid Mech.* 83 (01) (1977) 97–117.
- [45] I. Krieger, T. Dougherty, A mechanics for non-Newtonian flow in suspensions of rigid spheres, *Trans. Soc. Rheol.* 3 (1959) 137–152.
- [46] T. Kitano, T. Kataoka, T. Shiota, An empirical equation of the relative viscosity of polymer melts filled with various inorganic fillers, *Rheol. Acta.* 20 (1981) 207–209.
- [47] M. Abareshi, S.H. Sajjadi, S.M. Zebarjad, E.K. Goharshadi, Fabrication, characterization, and measurement of viscosity of α -Fe₂O₃-glycerol nanofluids, *J. Mol. Liq.* 163 (1) (2011) 27–32. doi:10.1016/j.molliq.2011.07.007.
- [48] M. Kole, T.K. Dey, Effect of aggregation on the viscosity of copper oxide-gear oil nanofluids, *Int. J. Therm. Sci.* 50 (9) (2011) 1741–1747. doi:10.1016/j.ijthermalsci.2011.03.027.
- [49] C.T. Nguyen, F. Desgranges, N. Galanis, G. Roy, T. Maré, S. Boucher, et al., Viscosity data for Al₂O₃ - water nanofluid - hysteresis: is heat transfer enhancement using nanofluids reliable?, *Int. J. Therm. Sci.* 47 (2) (2008) 103–111. doi:10.1016/j.ijthermalsci.2007.01.033.
- [50] S. Hosseini, A. Moghadassi, D.E. Henneke, A new dimensionless group model for determining the viscosity of nanofluids, *J. Therm Anal Calorim.* 100 (2010) 873–877. doi:10.1007/s10973-010-0721-0.
- [51] K. Khanafer, K. Vafai, A critical synthesis of thermophysical characteristics of nanofluids, *Int. J. Heat Mass Transf.* 54 (19-20) (2011) 4410–4428. doi:10.1016/j.ijheatmasstransfer.2011.04.048.
- [52] A.G. Ivakhnenko, The group method of data handling—a rival of the method of stochastic approximation, *Sov. Autom. Control.* 13 (3) (1966) 43–55.
- [53] M. Mehrabi, M. Sharifpur, J.P. Meyer, Application of the FCM-based neuro-fuzzy inference system and genetic algorithm-polynomial neural network approaches to modelling the thermal conductivity of alumina-water nanofluids, *Int. Commun. Heat Mass Transf.* 39 (2012) 971–997.
- [54] S. Atashrouz, G. Pazuki, Y. Alimoradi, Estimation of the viscosity of nine nanofluids using a hybrid GMDH-type neural network system, *Fluid Phase Equilib.* 372 (2014) 43–48. doi:10.1016/j.fluid.2014.03.031.

Figure Captions

Fig. 1 Experimental setup (a) sample preparation using ultrasonication (b) viscosity measurement setup

Fig. 2 TEM image and particle size distribution of Al_2O_3 nanoparticles (a) and (b) 19 nm (c) and (d) 139 nm (e) and (f) 160 nm

Fig. 3 X-Ray Diffraction pattern for Al_2O_3 nanoparticles (a) 19 nm (b) 139 nm (c) 160 nm

Fig. 4 UV-vis spectra analysis of Al_2O_3 -glycerol nanofluids (a, b and c) spectra pattern at different volume fraction and wavelength for 19, 139 and 160 nm respectively; (d, e and f) absorbance of Al_2O_3 in glycerol at different concentration and 230 nm wavelength for 19, 139 and 160 nm respectively

Fig. 5 Effect of ultrasonication energy density on effective viscosity (a) 2% volume fraction (b) 3% volume fraction

Fig. 6 Dependence of effective viscosity of Al_2O_3 -glycerol nanofluids on temperature (a) 19 nm (b) 139 nm (c) 160 nm

Fig. 7 Normalized viscosity of Al_2O_3 -glycerol nanofluids with varying volume fraction at different temperature (a) 19 nm (b) 139 nm (c) 160 nm

Fig. 8 Relative viscosity-volume fraction curve of Al_2O_3 -glycerol nanofluids

Fig. 9 Parity plot between the dimensional analysis model predictions and experimental data

Fig. 10 Comparison of experimental relative viscosity of Al_2O_3 -glycerol nanofluids with relative viscosity obtained from various model equations as a function of volume fraction (a) 19 nm (b) 139 nm (c) 160 nm

Fig. 11 Parity plot between the experimental relative viscosity of Al_2O_3 -glycerol nanofluid and GMDH-NN predicted results

Fig. 12 GMDH-NN performance in predicting the Al_2O_3 -glycerol viscosity data (a) effective viscosity vs temperature (b) relative viscosity vs volume fraction

Table 1 Statistics on the accuracy of models

Statistical parameters	Dimensional analysis model	GMDH-NN model
R ²	0.9495	0.9905
RMSE	0.1094	0.0447623
SSE	1.5310	-
MAE	-	0.0346317

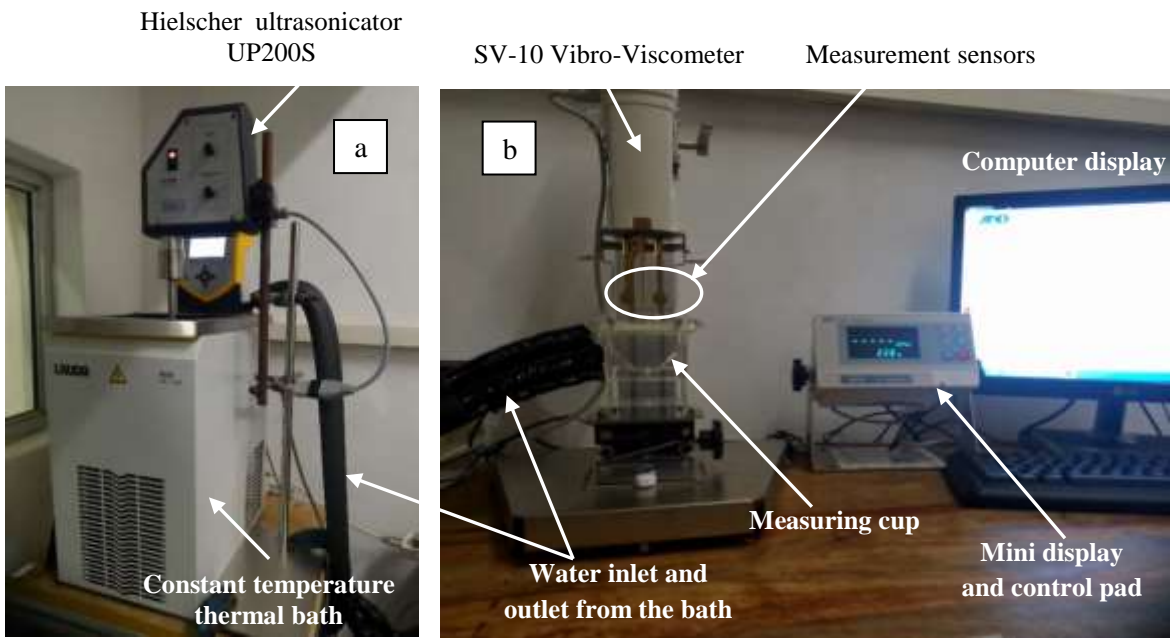


Fig. 1

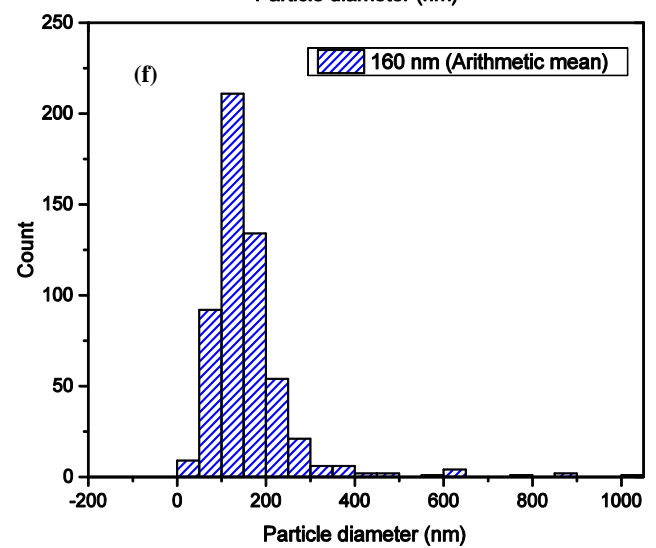
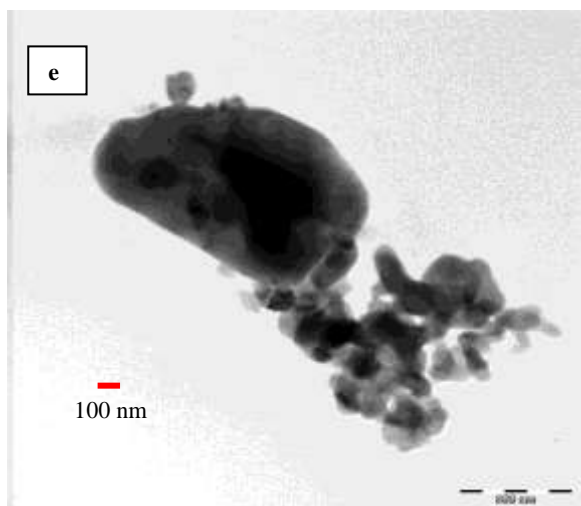
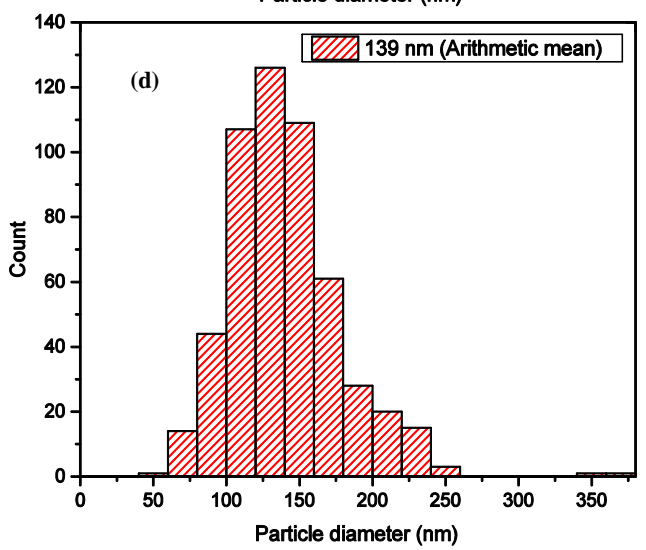
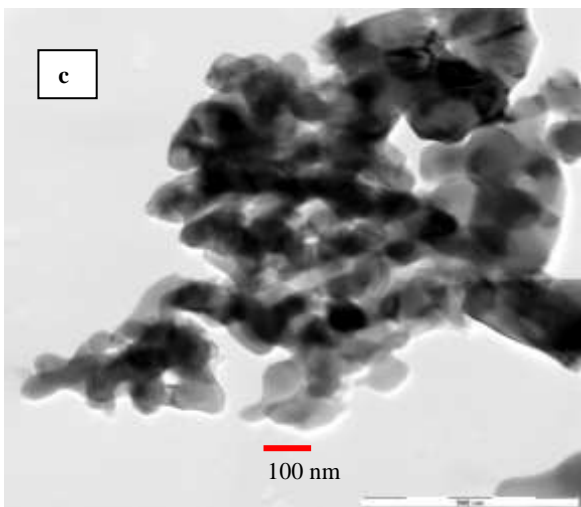
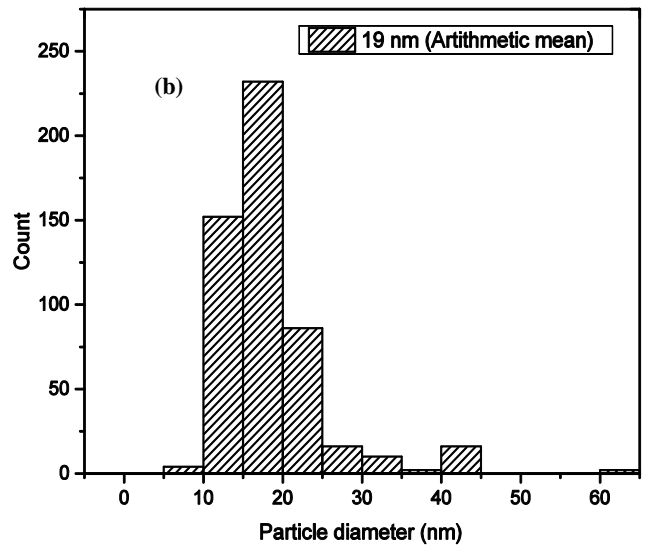
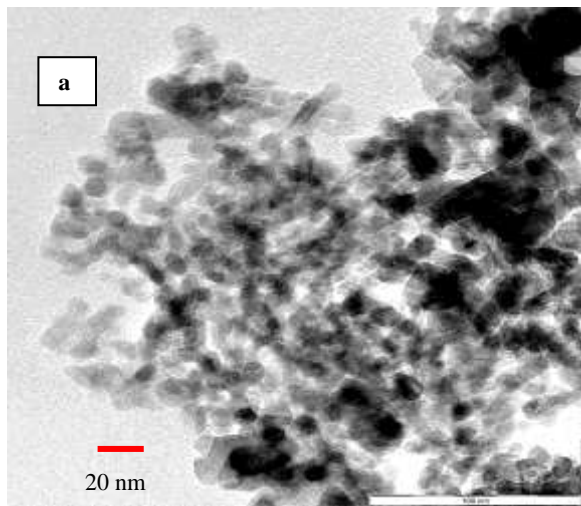


Fig. 2

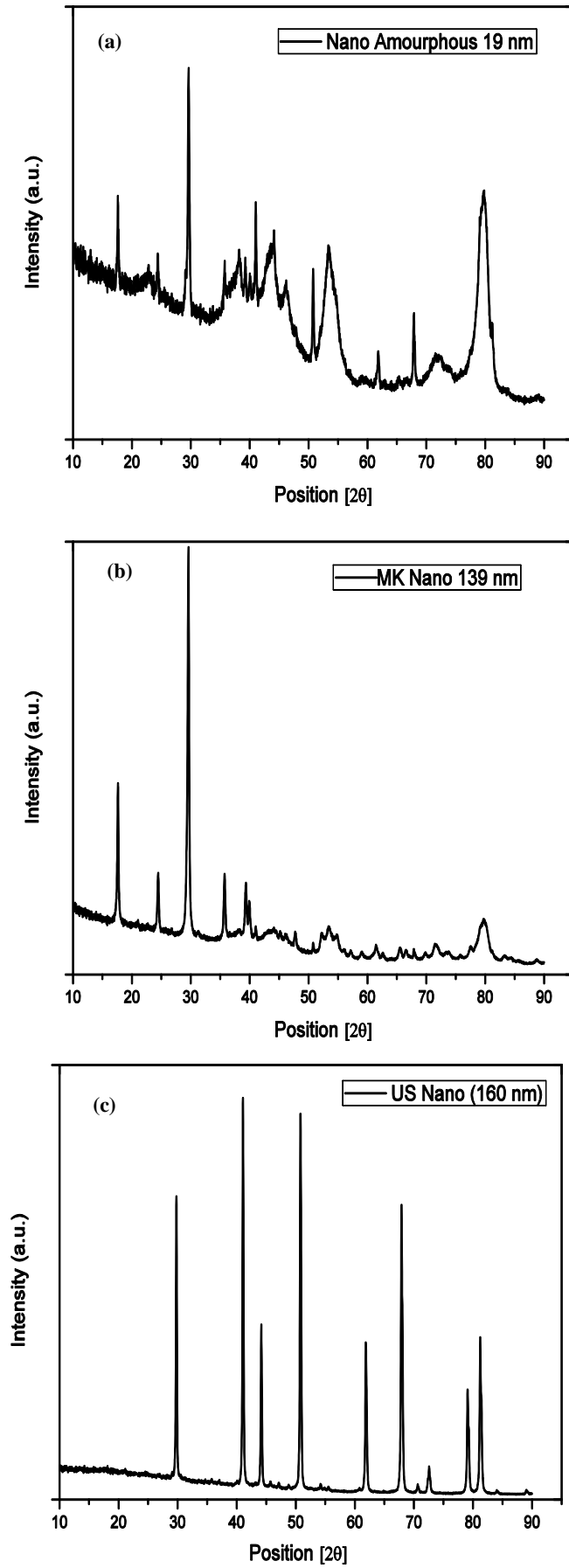


Fig. 3

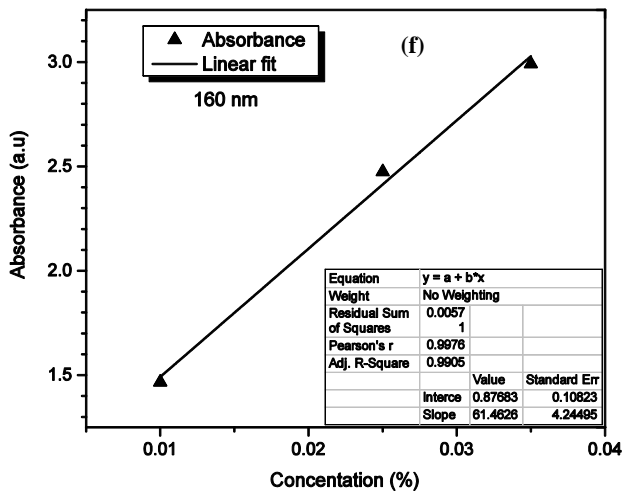
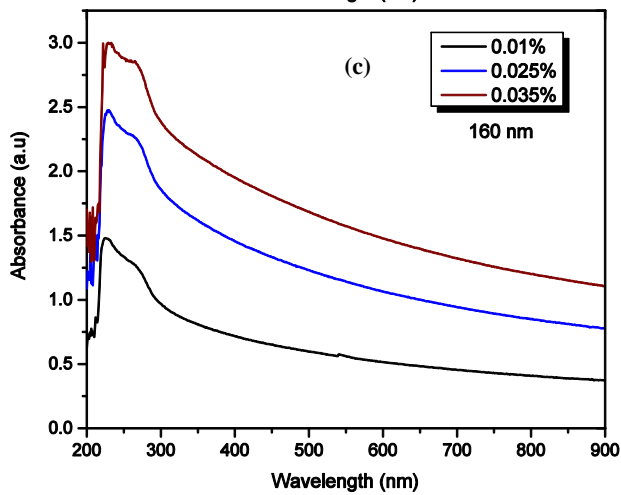
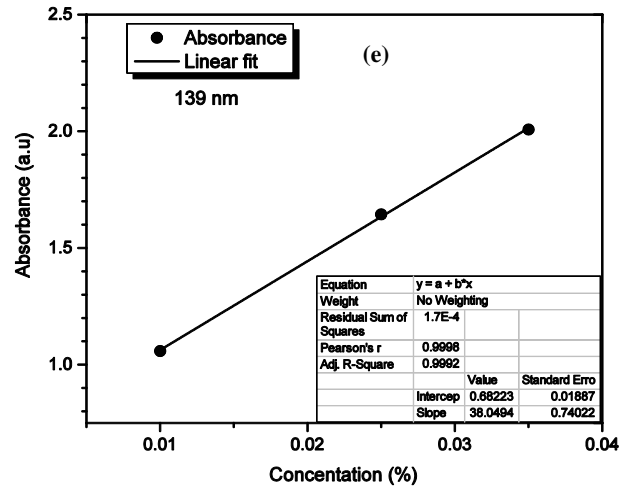
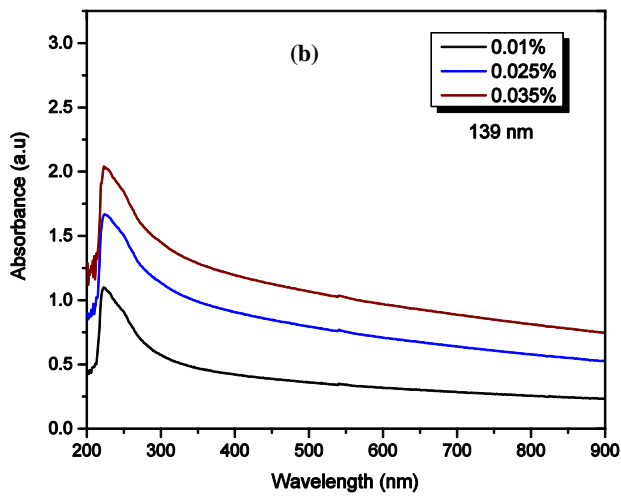
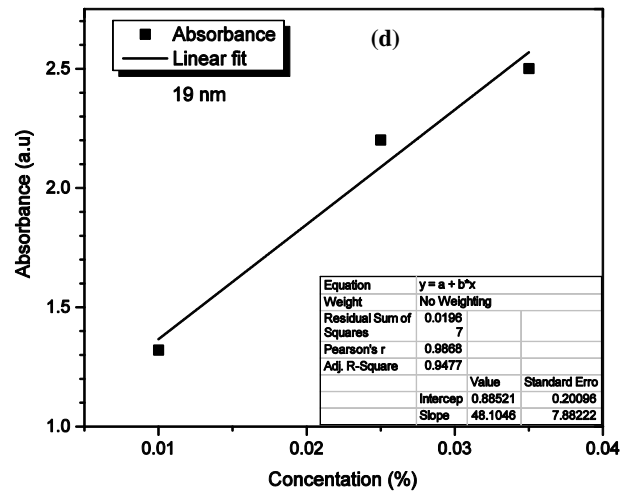
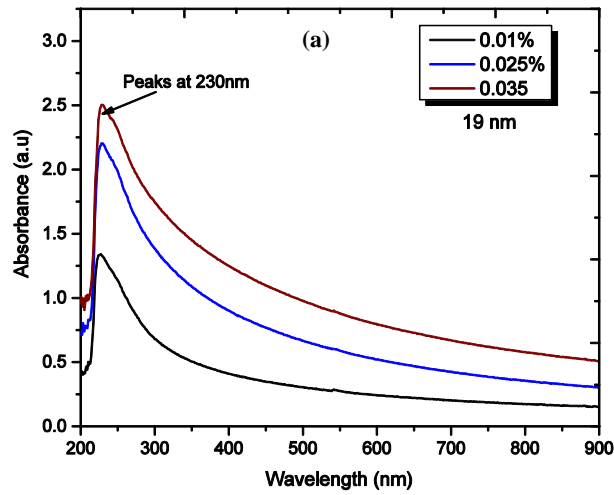


Fig. 4

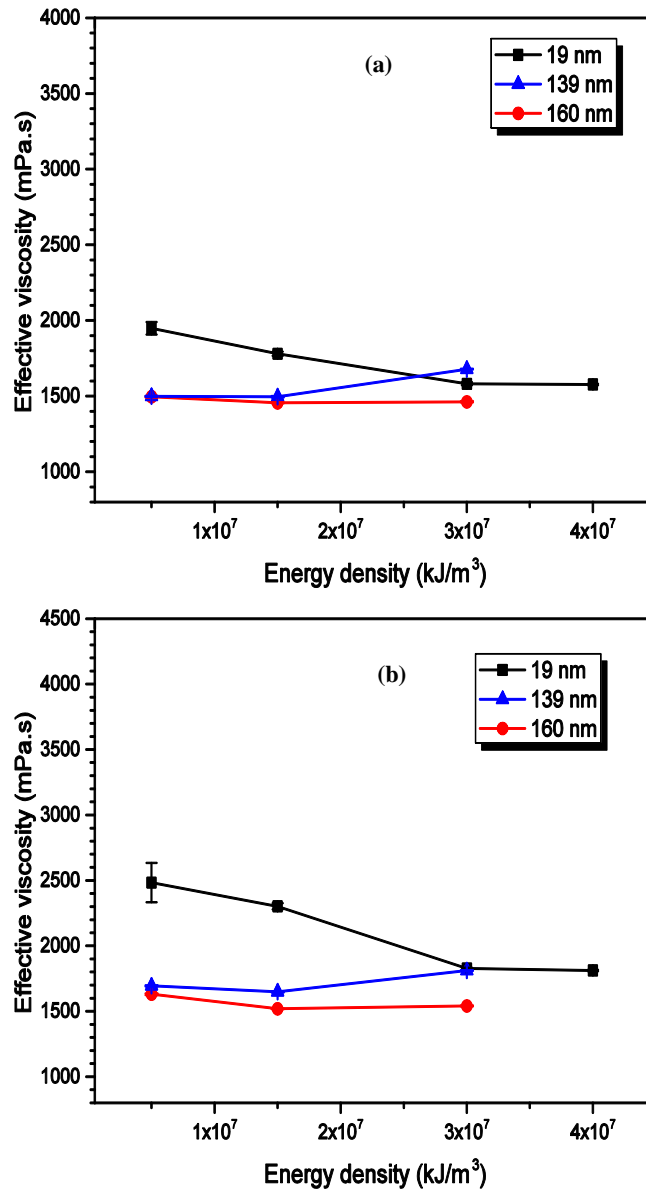


Fig. 5

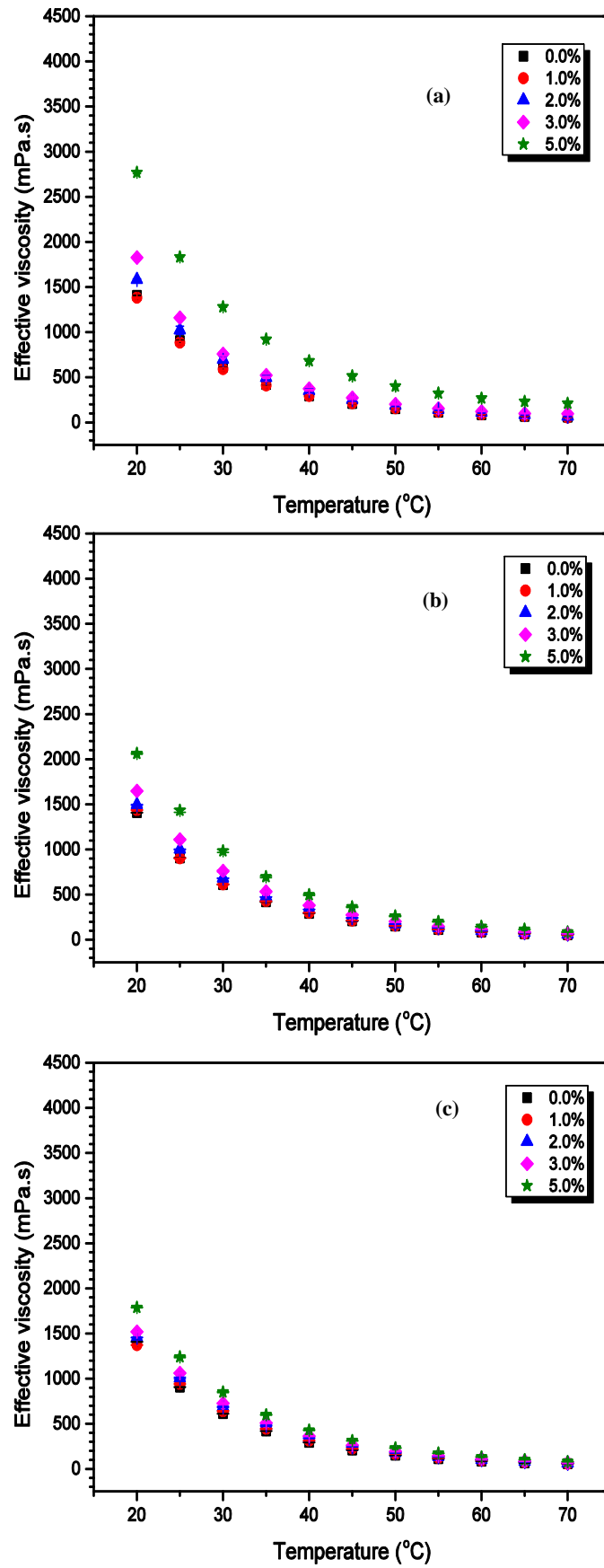


Fig. 6

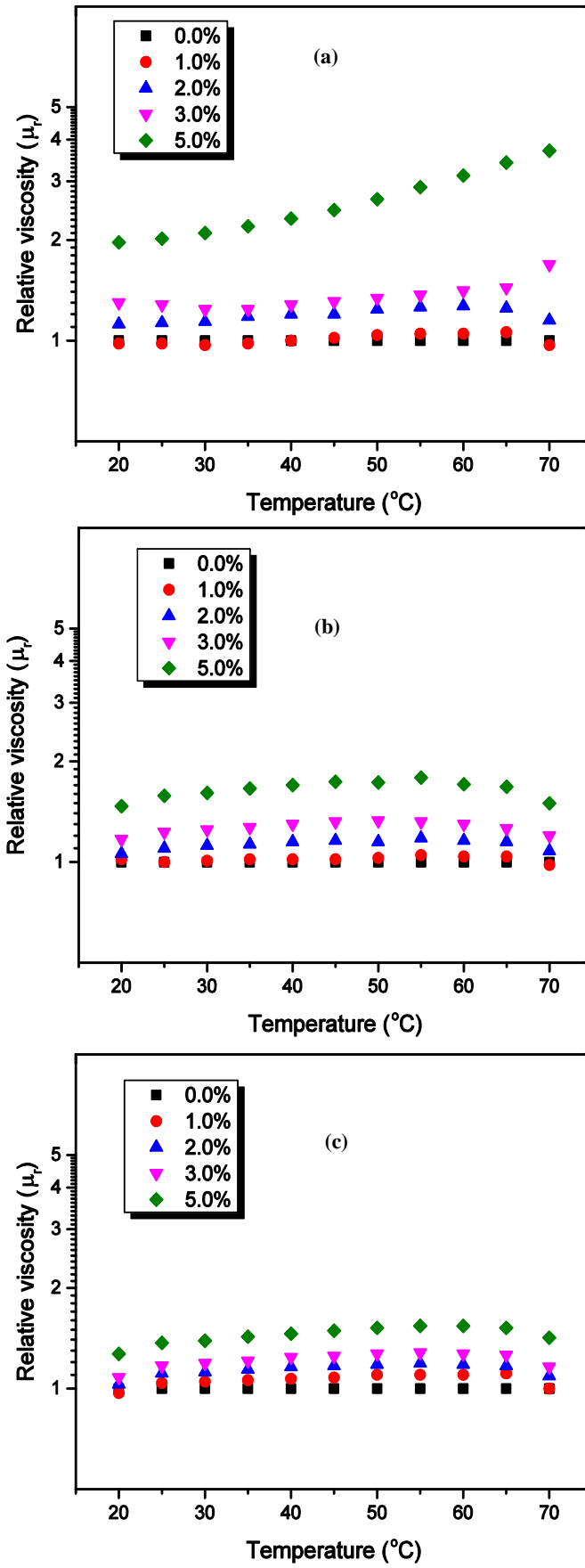


Fig. 7

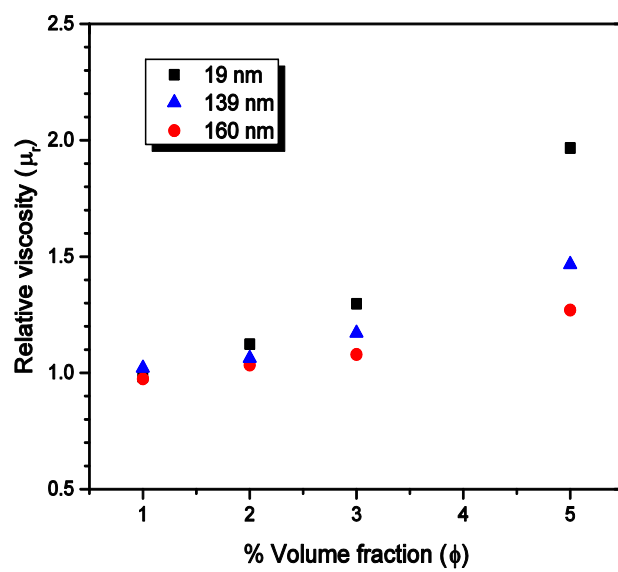


Fig. 8

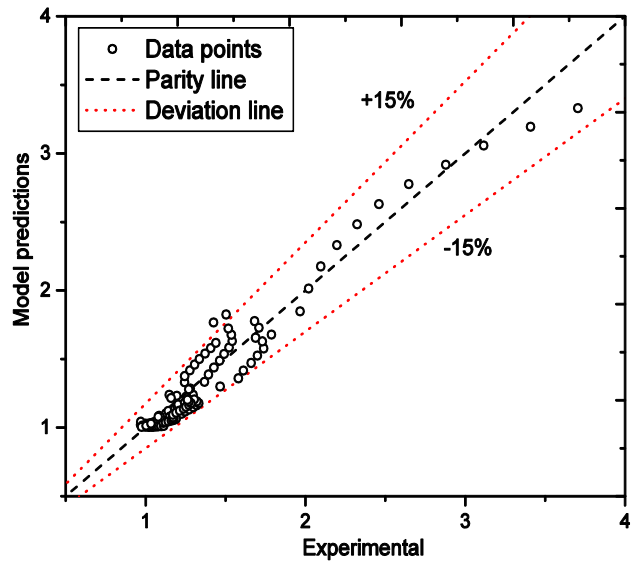


Fig. 9

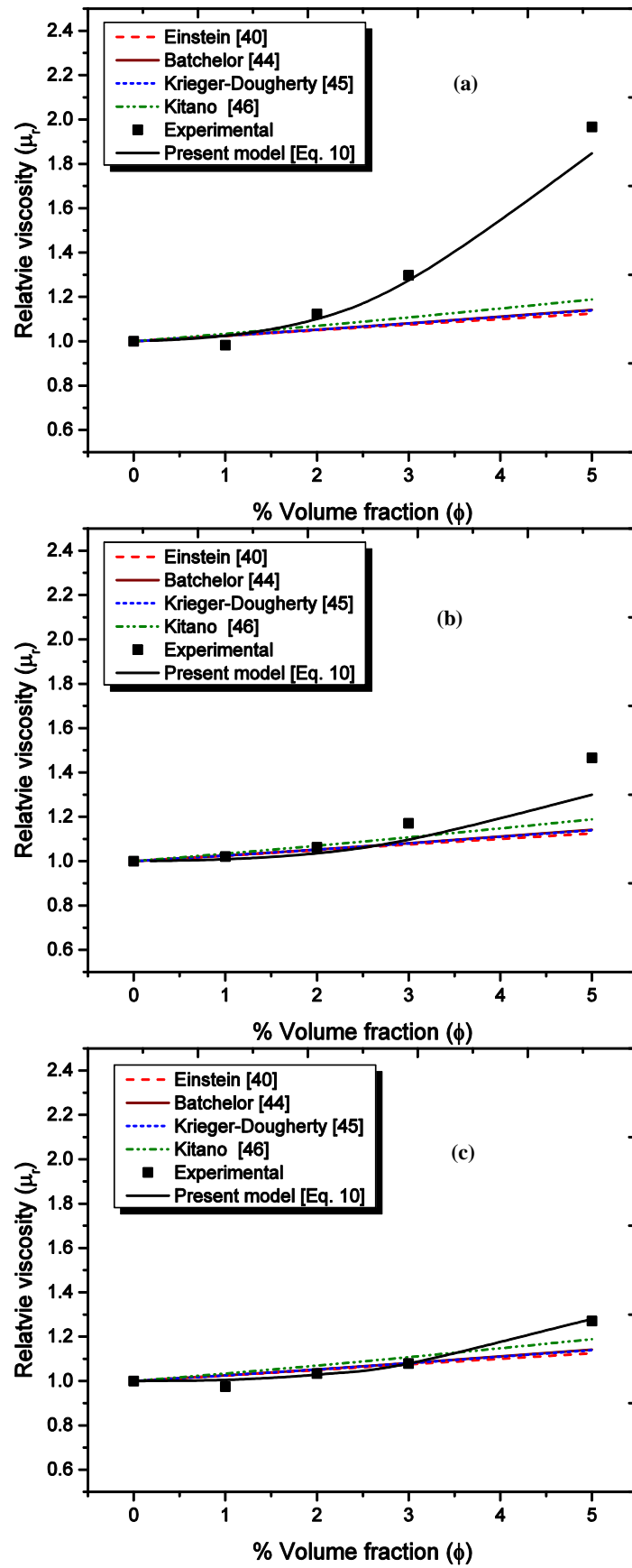


Fig. 10

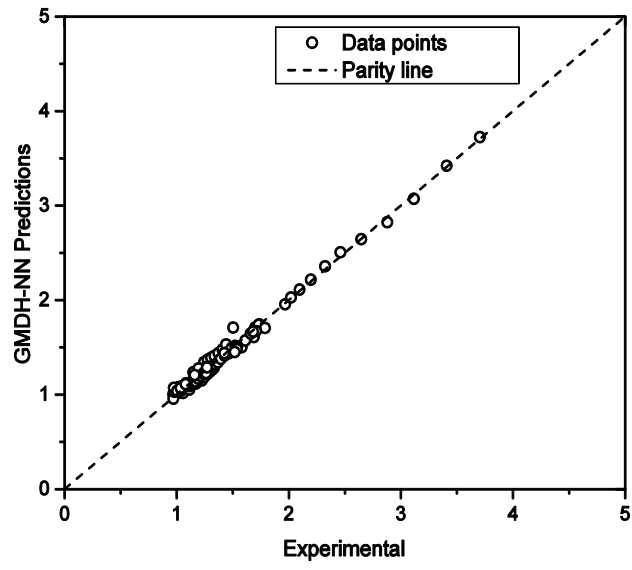


Fig. 11

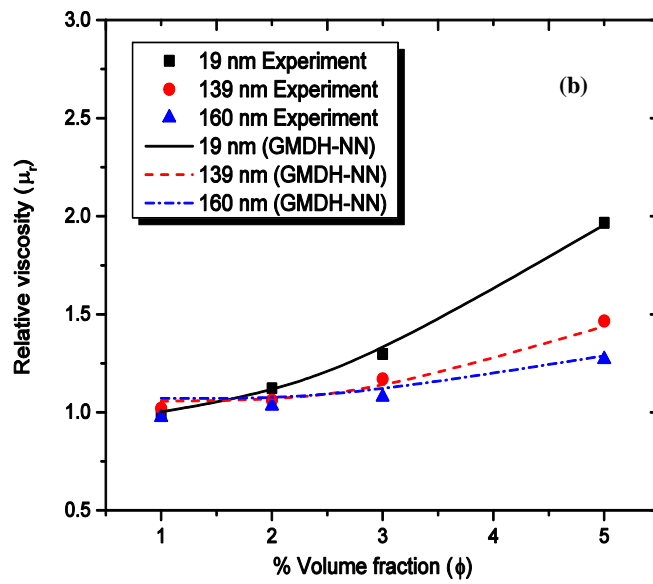
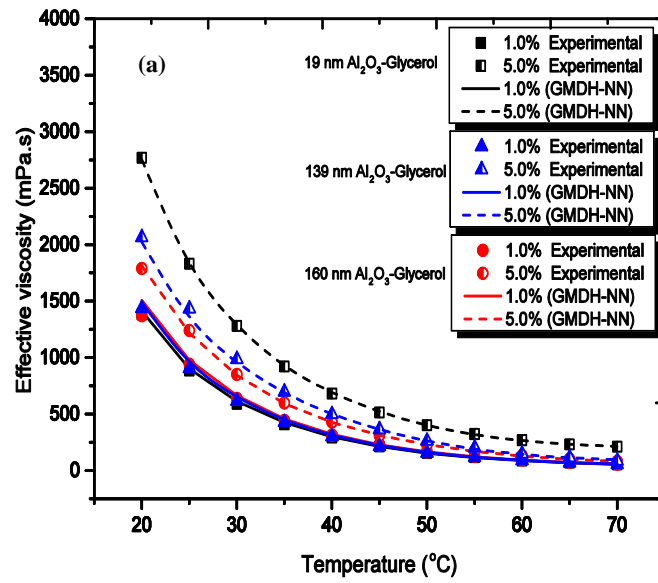


Fig. 12